Desalination and Water Treatment
www.deswater.com

doi: 10.5004/dwt.2018.21966

108 (2018) 345–352
March

Application of nanosilica-based adsorbent for the removal of rhodamine B and methylene blue from aqueous solutions

Akbar Eslami[a], Mohammad Mehralian[b], Zahra Godarzvand Chegini[c], Maryam Khashij[b,d,*]

[a]*Environmental and Occupational Hazards Control Research Center, Shahid Beheshi University of Medical Sciences, Tehran, Iran, Tel. +982122432040; email: aeslami@sbmu.ac.ir*
[b]*Department of Environmental Health Engineering, Kermanshah University of Medical Sciences, Kermanshah, Iran, Tel. +98 9364820423; email: m.khashij@yahoo.com (M. Khashij), Tel. +989132889214; email: mohammadmehralian@yahoo.com (M. Mehralian)*
[c]*Department of Environmental and Engineering, Islamic Azad University, Science and Research Branch, Tehran, Iran, Tel. +989132889312; email: chegini.azad@gmail.com*
[d]*Environmental Science and Technology Research Center, Department of Environmental Health Engineering, Shahid Sadoughi University of Medical Sciences, Yazd, Iran*

Received 15 March 2015; Accepted 28 January 2018

ABSTRACT

In this study, an adsorbent based on nanosilica molecules was synthesized by chemical activation and changing the structure of a sodium silicate)Na_2SiO_3(. The adsorbent was characterized by scanning electron microscope/energy-dispersive X-ray spectroscope, X-ray diffraction analysis, transmission electron microscope, and Brunauer–Emmett–Teller analysis for morphologic properties and determination of specific surface area. Sorption experiments were carried out to evaluate the effects of variables, such as initial dye concentration, contact time, and pH on the dye removal. Different isotherm and kinetic models were used to evaluate the sorption equilibrium and describe the sorption process. More than 75% removal efficiency was obtained within 15 min at adsorbent dose of 10 g/L for initial dye concentration of 150 mg/L. The maximum sorption capacity was found to be 92.9 mg/g at pH 10 and 70.9 mg/g at pH 9 for RB and MB, respectively. The best fit was achieved by the Langmuir isotherm equation (R^2 values = 0.99 and 0.98) for RB and MB, respectively. The kinetic studies showed that the RB and MB dye sorption onto the nanoadsorbent was best described by the pseudo-second-order kinetic model. This study showed that the sodium silicate nanoadsorbent can be an ideal adsorbent for dye removal and may also be used in environmental research in other fields.

Keywords: Adsorption; Nanosilicate; Rhodamine B; Methylene blue; Isotherm

1. Introduction

Many industries such as printing, textile, pharmaceutical, and food use different colored dyes in various applications to prepare products. Owing to continuous discharge of effluent from processing plants into the water stream, the presence of pollutants, toxins, and carcinogens in the environment is a serious issue [1]. Two of the commonly used industrial colorants that are soluble in water are rhodamine B (RB) and methylene blue (MB). Because of their carcinogenic nature, the entrance of RB and MB into the environment and subsequently the food chain is a threat to human health [2]. Illegal discharges spurred by low social awareness or lack of concern for their environmental impact have been reported [3]. Recently, different chemical or physical methods such as chemical or electrochemical oxidation, photocatalytic processes, and

* Corresponding author.

adsorption by natural or synthetic adsorbents have been used to treat colored wastewater. Among these methods, adsorption is the most developed method of dye removal because of the low cost of operation, high efficiency, and low impact on the environment [4]. Different natural and synthetic materials such as active carbon, zeolite, bentonite, modified jute, and biomaterials have been used as adsorbents [5–7]. With the development of nanotechnology to directly improve different processes, nanomaterials with high surface areas have been used to increase the concentration of adsorbed dyes and to ensure high removal rates of these dyes [8]. However, there have been demands for cost-effective technologies for the removal of dye from colored wastewater. As a result, sodium silicate nanomaterials, a series of metal silicates, have attracted the interest of researchers owing to their highly effective scavenging of pollutants. Many researchers have investigated various methods for preparing suitable silicate nanoadsorbents [8–10]. Recently, Tian et al. [2] prepared magnesium silicate magnetic hierarchical nanotubes (MSMHNs). Because of their excellent features, MSMHNs have been chosen as the carbon-assisted adsorbents for fast removal of cationic dyes [2]. Sodium silicate is a high-molecular weight compound that is also an effective scavenger of pollutants [11]. Owing to the large number of pores in the sodium silicate structure, it can adsorb pollutants through its stacking interaction. A literature review shows that there have been no reports on the use of sodium silicate nanoadsorbent for the removal of organic dye pollutants from aqueous solutions. The present study deals with the preparation and characterization of sodium silicate nanoadsorbent by a simple technique (chemical activation) and its application on the adsorption and determination of adsorption isotherms with various dyes such as RB and MB. The structural and physicochemical properties of the adsorbent were also characterized.

2. Materials and methods

2.1. Materials

The dyes, MB and RB, were purchased from Merck Company, Germany. The dye solutions of various concentrations (10, 20, 30, 50, 100, and 150 mg/L) in all experiments were prepared from a stock solution with a defined concentration of 1,000 mg/L. Using 0.1 M of HCl and NaOH from Merck Company, Germany, the pH of the solutions was adjusted to values between 5 and 12.

2.2. Synthesis of silica nanoadsorbent

To prepare the silica adsorbent, a sodium silicate (Na_2SiO_3) solution with specific weight of 1.35–1.36 g/mL (Merck, Germany) was mixed with water in a volume ratio of 1:3; the mixture was agitated by a mechanical stirrer at 1,000 rpm at 20°C ± 5°C (room temperature) for 20 min. After dispersion of the powder in water, the volume of the solution reached 1 L. To form nanometer-sized particles, 65% hydrochloric acid (Merck, Germany) was added to the mixture in a volume ratio of 1:10, to obtain a 15% solution of the original sodium silicate solution in a container made of polyethylene. The precipitated SiO_2 was heated for 10 min and then cooled at room temperature. Finally, the precipitated SiO_2 was separated and washed with distilled water. The separated precipitated SiO_2 was dried in a cyclone dryer based on the method of reverse isotope dilution analysis [12].

2.3. Characterization of silica nanoadsorbent

The X-ray diffraction (XRD) spectrum of the silica nanoadsorbent was recorded with a diffractometer (PW171/00, Philips, The Netherlands) and the adsorbent was prepared as KBr pellets. Images of the adsorbent were obtained with a scanning electron microscope (SEM; XI-30 ESEM-FEG, Philips, The Netherlands) using Cu-coated samples. The specific surface area of the adsorbent (Brunauer–Emmett–Teller analysis) was performed on a surface-area analyzer (SA-9600, Horiba, Japan).

2.4. Adsorption experiments

The experiments for dye removal were conducted in a batch reactor with a volume of 100 mL. First, 0.1 g of the silica nanoadsorbent was shaken in 100 mL dye solutions with different concentrations (10, 20, 30, 50, 100, and 150 mg/L) at 25°C. After this stage, the effect of variables such as nanoadsorbent dosage (10, 20, 30, 40, and 50 g/L) and time (5, 10, 15, 20, 30, 40, and 50 min) was determined. To determine the final concentration of the dyes, the samples were centrifuged to separate the nanoadsorbent from the solution. The UV–vis absorption spectroscopy was recorded using a Hatch 1600 PC spectrometer. The final concentration of a dye in a sample was determined by absorbance measurements at 562 and 663 nm for RB and MB, respectively, based on standard methods for water and wastewater examination [13]. The adsorption capacity was calculated using Eq. (1):

$$q_t = \frac{(C_0 - C_t)V}{W} \tag{1}$$

where q_t is the adsorption capacity of RB and MB at a particular time t (min), C_0 and C_t are the concentrations of the dye (mg/L) before and after adsorption, respectively. V is the volume of the solution (L), and W is the mass (g) of the dry adsorbent.

2.5. Isotherms and kinetic modeling

Isotherm models are commonly used to describe the equilibrium of adsorption process and behavior of the adsorbate and adsorbent in the liquid and solid phases. The Langmuir and Freundlich equations can be expressed as follows [14], respectively.

$$q_e = \frac{K_L q_{\max} C_e}{1 + K_L C_e}, \tag{2}$$

$$\log q_e = \log K_f + \frac{1}{n}\log C_e \tag{3}$$

where q_e is the equilibrium concentration of the nanoadsorbent (mol/g), K_L is the Langmuir constant, $q_{\max}$ is the maximum adsorption capacity of the nanoadsorbent (mol/g),

C_e is the equilibrium concentration of the dye in the solution (mol/L), K_f [(mg g^{-1}) (L/g)$^{-1/n}$] and n is the Freundlich constant that is related to the adsorption capacity and intensity. On the other hand, kinetics modeling of an adsorption system provides useful data regarding the adsorption efficiency and the feasibility of operations [15]. Kinetic modeling can be performed by using the pseudo-first-order model (Eq. (4)), which is also known as the Lagergren model [16], the pseudo-second-order model (Eq. (5)) [17], or the intraparticle diffusion model (Eq. (6)) [18]:

$$\log(q_e - q_t) = \log(q_e) - \frac{k_1 t}{2.303} \tag{4}$$

$$\frac{t}{q_t} = \left[\frac{1}{k_2 q_e^2}\right] + \frac{1}{q_e} t \tag{5}$$

$$q_t = k_i t^{0.5} + C_i \tag{6}$$

where q_t is the amount of dye adsorbed by the adsorbent during time t, q_e is the amount of dye adsorbed by the adsorbent (mg/g) in the equilibrium state, and k_1 is the constant for the first-order model (min^{-1}). k_1 represents the slope of the first-order equation and q_e stands for the intercept. In Eq. (5), k_2 is the constant for the pseudo-second-order model (mg/(g min)). The values of k_2 and q_e in the second-order kinetic model are determined from the slope and intercept of the plot of t/q_t vs. time. The model represented by Eq. (6) identifies the limiting step as a possible mechanism, where k_i is the intraparticle diffusion constant (mg/(g $min^{0.5}$)), and C_i is the intercept. This model is based on the assumption that intraparticle diffusion is the rate-limiting parameter in the adsorption process [18].

3. Results and discussion

3.1. Characterization of silica nanoadsorbent

The morphology of the silica nanoadsorbent, hereafter abbreviated as nanosilica, was analyzed by high-resolution SEM as shown in Fig. 1. The SEM images show that the synthesized nanoadsorbent had a uniformly rough and porous texture, and the thickness of the pore was approximately 500 nm. The average pore width and the total pore volume were high, which were favorable for dye adsorption [19]. The SEM images also show that the silica retained the original tubular structure, which agrees with the result reported by Qu et al. [11]. SEM analysis and energy-dispersive X-ray (EDX) spectroscopy were performed on the nanosilica. The EDX analysis results (Fig. 2) confirmed that the precipitated silica had high silicon content (70 wt%). They also confirmed that the silica was of high purity (99%) with free silicon. Furthermore, the EDX spectrum of the precipitated silica powder shows that it contained 99.9 wt% Si and 99.9 at% O. In addition, chemical analysis of the nanosilica confirms the absence of elements such as C, Cl, and Na, which is evidence of the formation of pure silica.

Transmission electron microscope (TEM; JEM-1400 TEM, JEOL, Japan) images were obtained at different parts of the

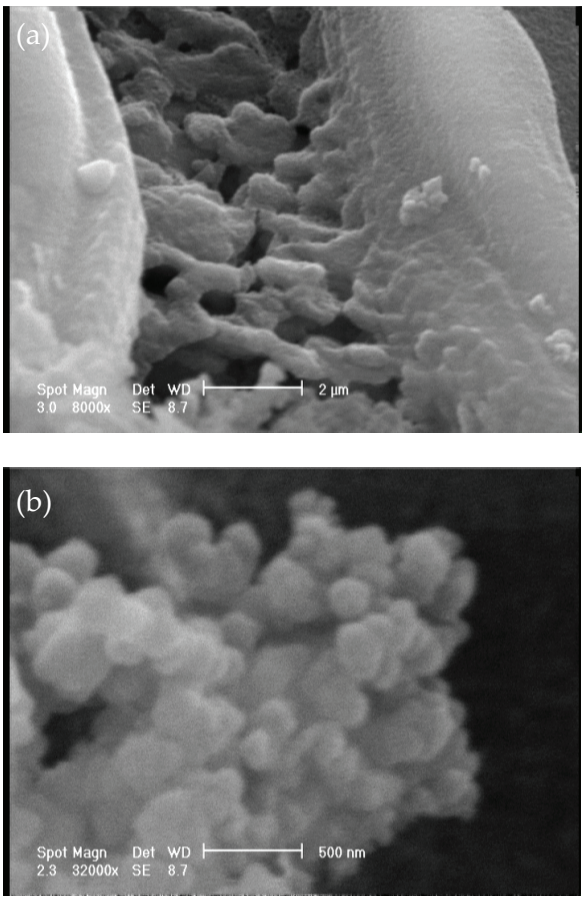

Fig. 1. SEM of silicate nanoadsorbents in 2 µm (a) and 500 nm (b).

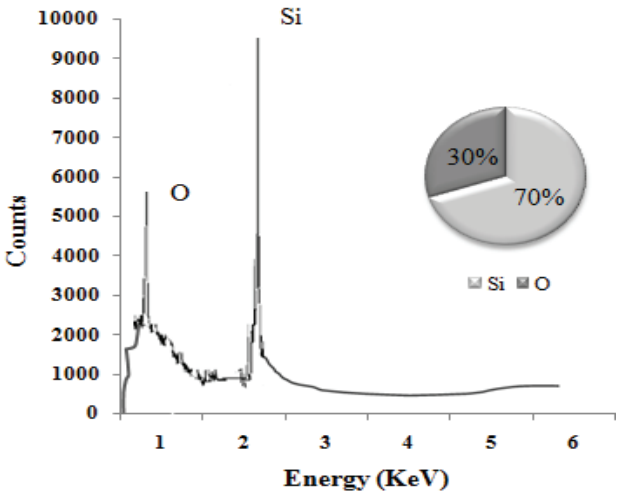

Fig. 2. EDX micrograph of silicate nanoadsorbents.

nanosilica. Fig. 3 shows that the mean particle size was 100 nm and the particles were almost spherical in shape. The mean diameter was 47.5 ± 9.3 nm (standard error of the mean).

The specific surface area of the nanosilica was 2,000 m^2/g. As a result of chemical activation and changing the structure of a sodium silicate (Na_2SiO_3), the bond between dyes and silica nanoparticles was improved, which could be related

to residual moisture desorption and the evaporation of the water molecules bound within nanoparticles [20]. The XRD spectrum of the nanoadsorbent in Fig. 4 clearly shows peaks between 10° and 100° that can be assigned to silicate. The peak at 2θ = 31° can be assigned to Si–O. Furthermore, analysis of the results indicates the functionalization of the silica nanoadsorbent by the adsorbed dye.

3.2. *Effect of pH on the RB–nanosilica and MB–nanosilica adsorption systems*

It is known that the adsorption of dye molecules on an adsorbent is affected by the solution pH [21]. Fig. 5 shows the adsorption of RB and MB on the nanoadsorbent at seven different pH levels. The adsorption of RB initially decreased as the pH increased and then increased when the pH reached 8. When the pH level was changed from acidic to alkaline, the removal of RB increased from 95.1% to 95.4% (Fig. 5) because of the competition between H^+ ions and the cationic dye at active sites on the nanoadsorbent [22]. As a result, lower amounts of RB were adsorbed in an acidic solution. As shown in Fig. 5, the amount of adsorbed MB greatly increased with increasing pH. As the pH changed from 4 to 9, the removal of MB increased from 99% to 99.5%, and subsequently decreased owing to the functional group in the structure of MB, which could dissociate with increasing solution pH [23]. Similar results were reported by Wang and Li [24] who stated that the decrease in MB removal occurred in an alkaline solution. Indeed, at an alkaline pH, some of the MB molecules

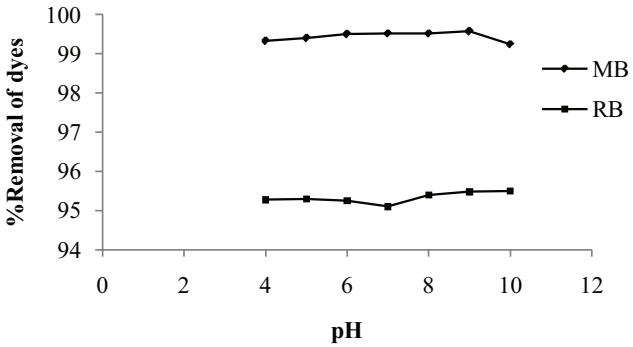

Fig. 5. Effect of pH on dyes removal.

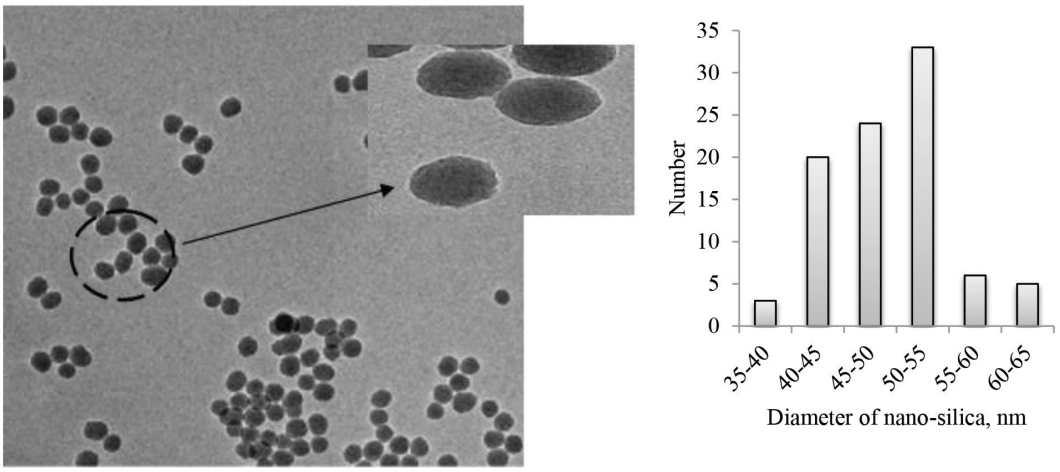

Fig. 3. TEM characterization of silicate nanoadsorbents (50 nm).

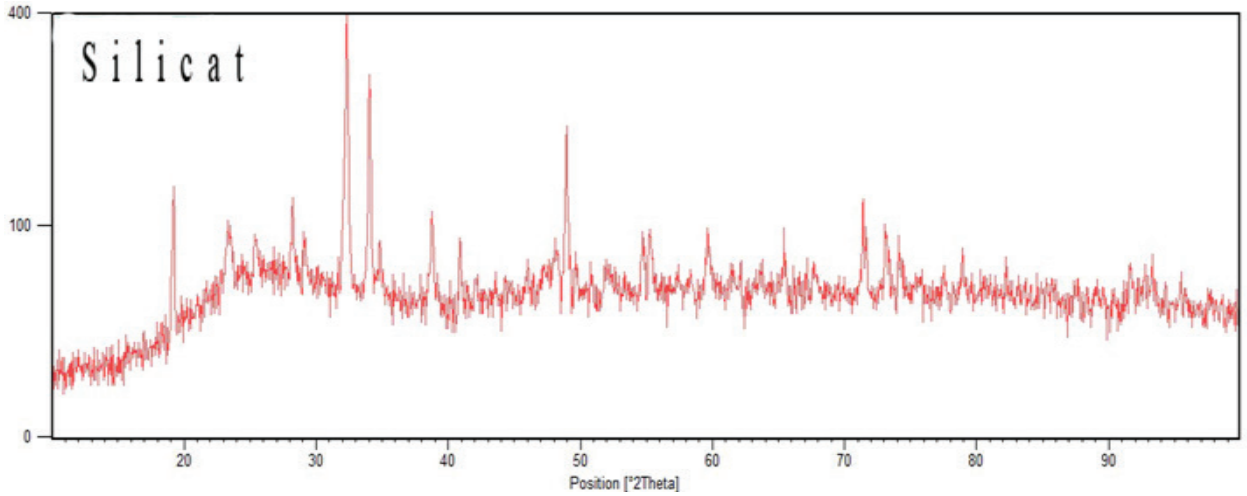

Fig. 4. XRD pattern of silicate nanoadsorbents.

were hydrolyzed on the adsorbent surface via the attached OH^-, and the MB molecules were eventually released from the nanoadsorbent. Therefore, the hydrolysis rate of molecules in a neutral or acidic solution was not noticeable. More importantly, MB played an anionic role at higher pH. Since there was sufficient electrostatic force between the negatively charged nanoadsorbent and the anionic MB, the dye adsorption greatly increased with increasing pH.

3.3. Effect of contact time on the RB–nanosilica and MB–nanosilica adsorption systems

Fig. 6 shows RB and MB adsorption on the silica nanoadsorbent at different times. Based on Fig. 6, it was observed that the adsorption of RB and MB onto adsorbent was relatively fast at initial time intervals, but with increasing the time, the dye adsorption amount increased slowly and gradually tended to equilibrium. The adsorption of RB and MB reached equilibrium after 40 min (Fig. 6). From Fig. 6, the amount of RB adsorbed at equilibrium was found to be 42.9 mg/g at the initial concentration of 100 mg/L. In the same conditions, the amount of MB adsorbed was 39.1 mg/g (Fig. 6). This time profile can be explained by monolayer adsorption on the adsorbent surface [25]. The porous structure of the silica nanoadsorbent and the small pores facilitated higher dye adsorption, which can be seen in Fig. 1. Similar results were reported for dye adsorption on different adsorbents, but the penetration of the adsorbate in the pores of the same adsorbent was reported to be low because of the larger sized molecules [26]. After the rapid adsorption, the adsorption quantity of dyes reached a constant value, which can be attributed to the electrostatic force between the negative charge of the nanoadsorbent and the positive charge of the dyes [27].

3.4. Effect of initial dye concentration on the RB–nanosilica and MB–nanosilica adsorption systems

The effect of dye concentration on its adsorption by the nanoadsorbent was investigated by adding different amounts of MB and RB from 10 to 150 mg/L at contact time of 15 min (Fig. 7). As shown in Fig. 7, the removal efficiency of RB and MB decreases with increase in initial concentration. The removal percentages of RB and MB were 98% and 93.2% in initial concentration of 10 mg/L, respectively. Also, at initial concentration of 150 mg/L, the removal percentage of RB and MB declined to 78. 6% and 75%, respectively. Liu et al. [25] conducted a study on removal of RB by tannic acid functionalized graphene and showed that by increasing the initial concentration of dye, the adsorption capacities decreased. This result was in agreement with the results reported in this study. Based on Fig. 7, the removal percentage of both dyes decreases slightly by increase of initial concentration indicating high adsorption capacity of the synthesized nanoadsorbent. Indeed, increasing the initial concentration of dyes, the number of active sites or surface area available decreases which consequently, decreases dye adsorption.

3.5. Adsorption isotherm model

An isotherm is used to demonstrate the equilibrium between the adsorbate in the liquid phase with the adsorbent, and an adsorption isotherm provides fundamental information regarding the interactive behavior of pollutants in the adsorption process [27]. There are several adsorption isotherm models [28,29]. Based on the literature, the adsorption of dyes usually follows the Langmuir isotherm [14], which is based on the assumption that monolayer adsorption takes place on a homogeneous adsorbent, where all the sites of adsorption are energetically equivalent. In the Langmuir model, one adsorbate molecule occupies a specific site and its likelihood to be adsorbed on the adsorbent surface is related to the free energy represented by the parameter K_L (i.e., the Langmuir constant) in Eq. (2) [30]. All sites of the adsorbent have the same tendency to adsorb an adsorbate molecule and after a complete monolayer of these molecules is adsorbed, this process reaches the maximum level (Table 1). As discussed in section 2.5, K_L can be calculated from the intercept of the plot of C_e/q_e vs. C_e, and the slope of the plot equals $1/q_{max}$. Q_m and K_f can also be calculated from the intercept and slope of $\log Q_e$ vs. C_e plot. Shajahan et al. [31] reported that the Langmuir model is the most appropriate isotherm to describe the behavior of RB on nanoparticles. They concluded that the RB uptake by the nanoparticles through the

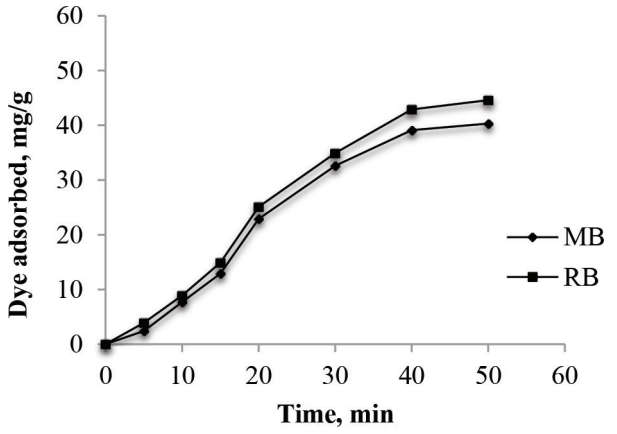

Fig. 6. Effect of contact time on dyes removal.

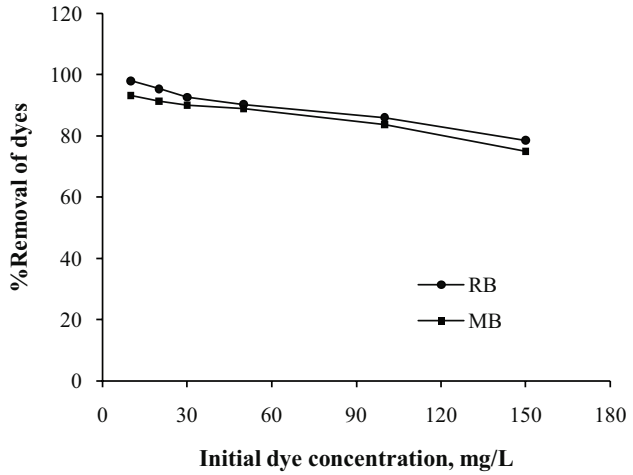

Fig. 7. Effect of initial dyes concentration. Time = 15 min, dosage of nanoadsorbent = 10 g/L.

Table 1
Isotherm parameters for adsorption of RB and MB

Dye	RB	MB
q_{max} (mg/g)	92.9	70.9
K_L (1/mg)	0.19	0.33
R^2	0.99	0.98
K_f (mg g^{-1}) (L mg^{-1})$^{1/n}$	47.05	32.1
$1/n$	0.14	0.19
R^2	0.88	0.84

electrostatic interactions between the dye molecules and the protonated functional groups in the nanoparticles contributed to Langmuir adsorption. In addition, the non-electrostatic interactions between RB and the nanoparticles contributed to partitioning. Besides, the equilibrium capacities of the nanoparticles for other dyes (MO, DR13, NBB, and CSB) followed the random adsorption theory.

Table 1 shows the parameters of Langmuir and Freundlich isotherms for the adsorption of RB and MB on the nanoadsorbent. Based on the regression coefficients, it can be concluded that significant dye adsorption took place. The maximum adsorption capacities for RB and MB were 92.9 and 70.9 mg/g, respectively, with the correlation coefficients (R^2) of 0.99 and 0.98, respectively. Regarding the values of the Langmuir constant (K_L), MB had a higher affinity to the nanoadsorbent as compared with RB (Table 1). Similar results were reported for the removal of RB and MB with AlMCM-41 adsorbent. Eftekhari et al. [32] also reported reversible adsorption on AlMCM-41. It is worthwhile considering that the size of MB is smaller than that of RB. Therefore, as compared with RB, the molecules of MB were mainly closely packed with the nanoadsorbent pores during the adsorption process, as confirmed by the K_L values of 0.19 and 0.33 mg^{-1} for RB and MB, respectively. In addition, the hydrolysis of RB molecules in aqueous systems can be caused by the renewed release of RB from the silica nanoadsorbent surface. However, the release of adsorbed MB from the active sites is supposed to be slower [24].

3.6. Adsorption kinetics model

As mentioned in section 2.5, kinetics modeling of adsorption is useful for providing data about the efficiency and feasibility of adsorption scale-up operations [15]. The kinetic model of adsorption can be based on constant speed, which is an important parameter when selecting material for the adsorption process. Fig. 8 shows the adsorption of MB and RB on the nanoadsorbent as a function of the contact time with the aqueous solution using the pseudo-first-order, pseudo-second-order, and intraparticle diffusion equations. As shown in the figure, the dye adsorption increased with increasing contact time. Maximum adsorption of RB and MB was obtained within almost 40 min. The equilibrium time was evaluated using different mathematical models.

The literature shows that when the adsorption conditions are far from equilibrium, the pseudo-first-order and pseudo-second-order models are widely used for kinetics modeling. The results of the adsorption kinetics and the parameters for the adsorption of RB and MB on

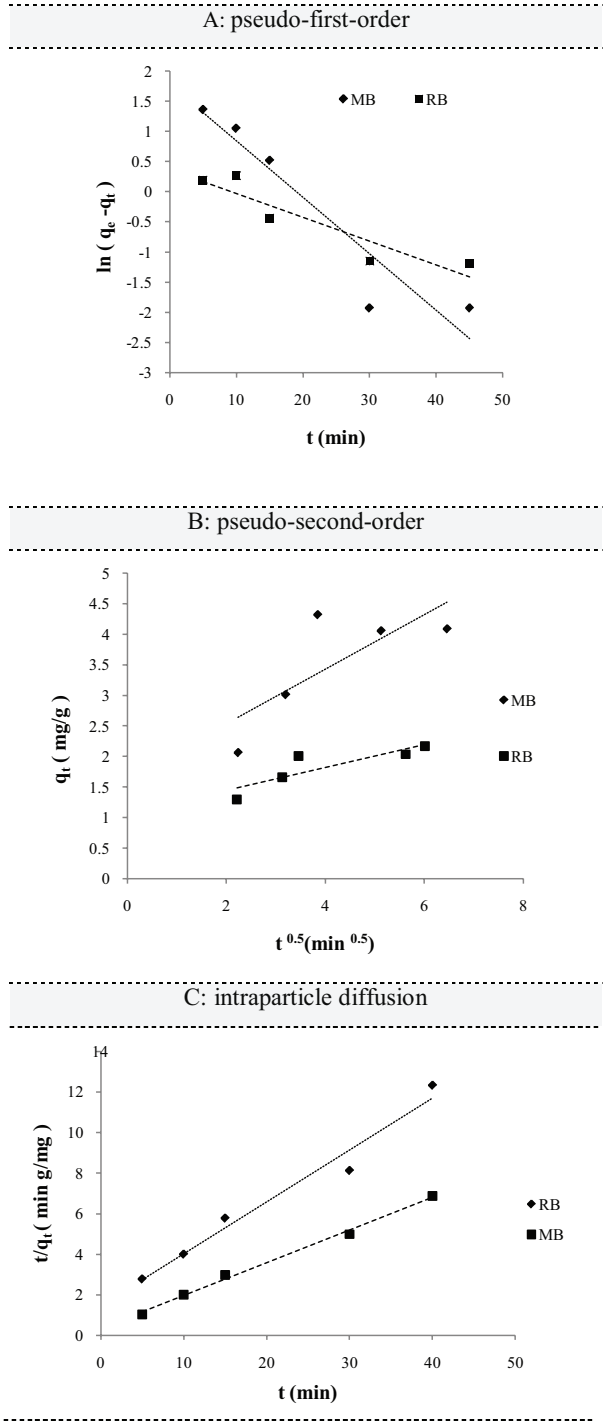

Fig. 8. Kinetic models for MB and RB adsorption onto silicate nanoadsorbents.

the nanoadsorbent are tabulated in Table 2, and their plots are shown in Fig. 8. The correlation coefficient (R^2) was calculated for the best fit. Table 2 shows that the adsorption kinetics of RB and MB can be well described by the pseudo-second-order model, with high R^2 of 0.99 and 0.98, respectively. Owing to the nature of MB molecules, makes it mostly absorbable on the nanoadsorbent surface, its correlation coefficient (0.99) is expected to be higher than that of MB

Table 2
Adsorption kinetics and the parameters for adsorption of RB and MB

Pseudo-first-order	Pseudo-second-order	Intraparticle diffusion
RB		
$y = –0.0396x + 0.369$	$y = 0.2561x + 1.473$	$y = 0.185x + 1.078$
$R^2 = 0.85$	$R^2 = 0.97$	$R^2 = 0.74$
MB		
$y = –0.0937x + 1.78$	$y = 0.1614x + 0.3445$	$y = 0.4452x + 1.6$
$R^2 = 0.89$	$R^2 = 0.99$	$R^2 = 0.59$

(0.98 comparatively 0.99). This was also due to the diffusion of RB molecules into the pores in the adsorbent. Therefore, it is very clear why the pseudo-second-order rate for MB adsorption on the silica nanoadsorbent was higher than that for the RB adsorption. As a result, a good relationship was obtained between the initial concentration of the dyes and the pseudo-second-order equation, and the values of q_e were consistent with the experimental results.

The value of R^2 for the intraparticle model was high. This model also showed a high C_i value, which was not a good sign because it should be close to zero. Besides, for RB and MB, the values of q_e calculated from the pseudo-second-order kinetic model fitted the experimental results. The kinetic plots of regression are shown in Fig. 8. The pseudo-second-order model is usually the best model for the adsorption of cationic dyes. The same behavior was reported by Tian et al. [2] for MB adsorption. In addition, it should be noted that the pseudo-first-order and pseudo-second-order kinetic models do not identify the diffusion mechanism of the dye into the nanoadsorbent. The data were thus analyzed by the intraparticle diffusion kinetic model to determine the diffusion mechanism [33]. As shown in the linear plot and kinetic parameters in Fig. 8, the model of intraparticle diffusion yielded a poor linear relationship for the initial concentration of MB and RB (R^2 = 0.59 and 0.74, respectively), which was lower than the correlation coefficient of the pseudo-second-order kinetic model for the adsorption process on the nanoadsorbent. Meanwhile, Fig. 8 indicates that even though the adsorption of both dyes involved intraparticle diffusion, this mechanism was not the only rate-controlling phase in the process. Therefore, Fig. 8 reveals that the pseudo-second-order kinetic model is the dominant one and parts of several models were involved in the rate of adsorption [34].

4. Conclusion

The silica nanoadsorbent was used for the adsorption of two dyes, RB and MB. The results indicated that the prepared nanoadsorbent was significantly capable of dye absorption, and the adsorption capacity for MB was higher than that for RB owing to the difference in their molecular structures. The maximal removal rates for RB and MB were 94.04% and 99.7%, respectively, for a dye concentration of 100 mg/L. For this system, the adsorption results were fairly well fitted by the Langmuir isotherm. The kinetics of the dye adsorption on the nanoadsorbent was better described by the pseudo-second-order model, with R^2 values of 0.99 and 0.98 for the adsorption of MB and RB, respectively. The adsorption of RB and MB also increased with increasing pH and subsequently decreased. Finally, the properties of the precipitated SiO_2 produced by neutralization of the sodium silicate solution and acid solution matched those obtained in the laboratory.

References

[1] Y. Zhang, J. Wang, L. Wang, R. Feng, F. Zhang, Study on adsorption properties of QCS/PS-G8-2-8 anion exchange membrane for Rhodamine B, J. Mol. Struct., 1089 (2015) 116–123.
[2] A. Tian, G. Cui, Y. Liu, H. Li, Z. Sun, S. Yan, Self-assembly synthesis of hollow double silica @ mesoporous magnesium silicate magnetic hierarchical nanotubes with excellent performance for fast removal of cationic dyes, Appl. Surf. Sci., 387 (2016) 631–641.
[3] A. Mehrdad, R. Hashemzadeh, Ultrasonic degradation of rhodamine B in the presence of hydrogen peroxide and some metal oxide, Ultrason. Sonochem., 17 (2010) 168–172.
[4] F. Tan, M. Liu, K. Li, Y. Wang, J. Wang, X. Guo, G. Zhang, C. Song, Facile synthesis of size-controlled MIL-100(Fe) with excellent adsorption capacity for methylene blue, Chem. Eng. J., 281 (2015) 360–367.
[5] Y. Hai, X. Li, H. Wu, S. Zhao, W. Deligeer, S. Asuha, Modification of acid-activated kaolinite with TiO_2 and its use for the removal of azo dyes, Appl. Clay Sci., 114 (2015) 558–567.
[6] M.S. Hassan, Removal of reactive dyes from textile wastewater by immobilized chitosan upon grafted jute fibers with acrylic acid by gamma irradiation, Radiat. Phys. Chem., 115 (2015) 55–61.
[7] S. Liu, Y. Ding, P. Li, K. Diao, X. Tan, F. Lei, Y. Zhan, Q. Li, B. Huang, Z. Huang, Adsorption of the anionic dye Congo red from aqueous solution onto natural zeolites modified with *N*,*N*-dimethyl dehydroabietylamine oxide, Chem. Eng. J., 248 (2014) 135–144.
[8] M. Khashij, A. Moheb, M. Mehralian, M. Gharloghi, Modeling of the adsorption breakthrough behaviors of 4-chlorophenol in a fixed bed of nano graphene oxide adsorbent, J. Water Supply Res. Technol. AQUA, 65 (2016) 127–134.
[9] Y. Yang, Y.A. Zhuang, Y.A. He, B. Bai, X. Wang, Fine tuning of the dimensionality of zinc silicate nanostructures and their application as highly efficient absorbents for toxic metal ions, Nano Res., 3 (2010) 581–593.
[10] Y.Q. Wang, G.Z. Wang, H.Q. Wang, W.P. Cai, L.D. Zhang, One-pot synthesis of nanotube-based hierarchical copper silicate hollow spheres, Chem. Commun., 65 (2008) 6555–6557.
[11] W. Qu, C.Y. Li, X. Cao, L. Yin, J. Zhao, Z. Bai, W.G. Qin, Metal silicate nanotubes with nanostructured walls as superb adsorbents for uranyl ions and lead ions in water, J. Mater. Chem., 22 (2012) 17222–17226.
[12] M.A. Rida, F. Harb, Synthesis and characterization of amorphous silica nanoparitcles from aqueous silicates using cationic surfactants, J. Met. Mater. Miner., 24 (2014) 37–42.
[13] APHA, Standard Methods for the Examination of Water and Wastewater, American Public Health Association (APHA), Washington, D.C., USA, 2005.
[14] M.A. Rauf, S.M. Qadri, S. Ashraf, K.M. Al-Mansoori, Adsorption studies of Toluidine Blue from aqueous solutions onto gypsum, Chem. Eng. J., 150 (2009) 90–95.
[15] S. Wang, H. Li, S. Xie, S. Liu, L. Xu, Physical and chemical regeneration of zeolitic adsorbents for dye removal in wastewater treatment, Chemosphere, 65 (2006) 82–87.
[16] R. Lafi, A. Ben Fradj, A. Hafiane, B. Hameed, Coffee waste as potential adsorbent for the removal of basic dyes from aqueous solution, Korean J. Chem. Eng., 31 (2014) 2198–2206.
[17] Y.S. Ho, G. McKay, Pseudo-second order model for sorption processes, Process Biochem., 34 (1999) 451–465.
[18] W.J. Weber, J.C. Morris, Kinetics of adsorption on carbon from solution, J. Sanit. Eng. Div., 89 (1963) 31–60.

[19] G. Cui, Z. Sun, H. Li, X. Liu, Y. Liu, Y. Tian, S. Yan, Synthesis and characterization of magnetic elongated hollow mesoporous silica nanocapsules with silver nanoparticles, J. Mater. Chem. A, 4 (2016) 1771–1783.
[20] C. Mulder, J. Van Lierop, Preparation, densification and characterization of autoclave dried SiO_2 gels, Aerogels, 2 (1986) 68–75.
[21] A.S. Patra, S. Ghorai, S. Ghosh, B. Mandal, S. Pal, Selective removal of toxic anionic dyes using a novel nanocomposite derived from cationically modified guar gum and silica nanoparticles, J. Hazard. Mater., 301 (2016) 127–136.
[22] F. Batzias, D. Sidiras, Simulation of dye adsorption by beech sawdust as affected by pH, J. Hazard. Mater., 141 (2007) 668–679.
[23] Y. Qin, L. Wang, C. Zhao, D. Chen, Y. Ma, W. Yang, Ammonium-functionalized hollow polymer particles as a pH-responsive adsorbent for selective removal of acid dye, ACS Appl. Mater. Interfaces, 8 (2016) 16690–16698.
[24] S. Wang, H. Li, Structure directed reversible adsorption of organic dye on mesoporous silica in aqueous solution, Microporous Mesoporous Mater., 97 (2006) 21–26.
[25] K. Liu, H. Li, H. Wang, X. Gou, Y. Duan, Adsorption and removal of rhodamine B from aqueous solution by tannic acid functionalized graphene, Colloids Surf., A, 477 (2015) 35–41.
[26] M. Khashij, S. Mousavi, M. Mehralian, M. Massoudinejad, Removal of Fe^{2+} from aqueous solution using manganese oxide coated zeolite and iron oxide coated zeolite, Int. J. Eng. Trans. B, 29 (2016) 1587–1594.
[27] W. Gao, S. Zhao, H. Wu, W. Deligeer, S. Asuha, Direct acid activation of kaolinite and its effects on the adsorption of methylene blue, Appl. Clay Sci., 126 (2016) 98–106.
[28] S. Wu, X. Shen, H. Zhou, G. Zhu, R. Wang, Z. Ji, K. Chen, C. Chen, Morphological synthesis of Prussian blue analogue $Zn_3[Fe(CN)_6]_2$ xH_2O micro-/nanocrystals and their excellent adsorption performance toward methylene blue, J. Colloid Interface Sci., 464 (2016) 191–197.
[29] L. Tang, Y. Cai, G. Yang, Y. Liu, G. Zeng, Y. Zhou, S. Li, J. Wang, S. Zhang, Y. Fang, Y. He, Cobalt nanoparticles-embedded magnetic ordered mesoporous carbon for highly effective adsorption of rhodamine B, Appl. Surf. Sci., 314 (2014) 746–753.
[30] R. Natrajan, Chromogenic polyaniline picrate – a novel sorbent for selectivity of anions in potassium and sodium salts, Indian J. Chem. Technol., 23 (2016) 104–113.
[31] A. Shajahan, S. Shankar, A. Sathiyaseelan, K.S. Narayan, V. Narayanan, V. Kaviyarasan, S. Ignacimuthu, Comparative studies of chitosan and its nanoparticles for the adsorption efficiency of various dyes, Int. J. Biol. Macromol., 104 (2017) 1449–1458.
[32] S. Eftekhari, A. Habibi-Yangjeh, S. Sohrabnezhad, Application of AlMCM-41 for competitive adsorption of methylene blue and rhodamine B: thermodynamic and kinetic studies, J. Hazard. Mater., 178 (2010) 349–355.
[33] S. Agarwal, I. Tyagi, V.K. Gupta, N. Ghasemi, M. Shahivand, M. Ghasemi, Kinetics, equilibrium studies and thermodynamics of methylene blue adsorption on *Ephedra strobilacea* saw dust and modified using phosphoric acid and zinc chloride, J. Mol. Liq., 218 (2016) 208–218.
[34] M. Szabo, Z. Baranyai, K.L. Somsak, I. Fabian, The decomposition of N-chloroglycine in alkaline aqueous solution: kinetics and mechanism, Chem. Res. Toxicol., 2 (2015) 1282–1291.